Mechanism research of elastic fixation promoting fracture healing based on proteomics and fracture microenvironment

From Tianjin Fourth Central Hospital, Tianjin, China

Cite this article:
Bone Joint Res 2024;13(10):
559–572.

DOI: 10.1302/2046-3758.
1310.BJR-2023-0257.R2

Correspondence should be sent to Yongqing Wang
13820789626@139.com

W. Wu,[1,2] Z. Zhao,[3] Y. Wang,[3] M. Liu,[3] G. Zhu,[4] L. Li[4]

[1]First Teaching Hospital of Tianjin University of Traditional Chinese Medicine, Tianjin, China
[2]National Clinical Research Center for Chinese Medicine Acupuncture and Moxibustion, Tianjin, China
[3]Orthopedic Department, The Fourth Central Clinical School, Tianjin Medical University, Tianjin, China
[4]General Clinical Research Center, Anhui Wanbei Coal-Electricity Group General Hospital, Suzhou, China

Aims

This study aimed to demonstrate the promoting effect of elastic fixation on fracture, and further explore its mechanism at the gene and protein expression levels.

Methods

A closed tibial fracture model was established using 12 male Japanese white rabbits, and divided into elastic and stiff fixation groups based on different fixation methods. Two weeks after the operation, a radiograph and pathological examination of callus tissue were used to evaluate fracture healing. Then, the differentially expressed proteins (DEPs) were examined in the callus using proteomics. Finally, in vitro cell experiments were conducted to investigate hub proteins involved in this process.

Results

Mean callus volume was larger in the elastic fixation group (1,755 mm^3 (standard error of the mean (SEM) 297)) than in the stiff fixation group (258 mm^3 (SEM 65)). Pathological observation found that the expression levels of osterix (OSX), collagen, type I, alpha 1 (COL1α1), and alkaline phosphatase (ALP) in the callus of the elastic fixation group were higher than those of the stiff fixation group. The protein sequence of the callus revealed 199 DEPs, 124 of which were highly expressed in the elastic fixation group. In the in vitro study, it was observed that a stress of 200 g led to upregulation of thrombospondin 1 (THBS1) and osteoglycin (OGN) expression in bone marrow mesenchymal stem cells (BMSCs). Additionally, these genes were found to be upregulated during the osteogenic differentiation process of the BMSCs.

Conclusion

Elastic fixation can promote fracture healing and osteoblast differentiation in callus, and the ability of elastic fixation to promote osteogenic differentiation of BMSCs may be achieved by upregulating genes such as THBS1 and OGN.

Article focus

- This study aimed to investigate the promoting effect of elastic fixation on fracture healing, and to identify the primary genes that function in this process.

Key messages

- Elastic fixation can promote the transformation of callus at the fracture site and osteoblast differentiation in the callus.
- The promoting effect of elastic fixation on fracture healing may be achieved through high thrombospondin 1 (THBS1) and osteoglycin (OGN) expression.

Strengths and limitations

- This study demonstrated the promoting effect of elastic fixation on fracture healing through animal experiments, and preliminarily identified the hub genes involved in this process through proteomics and in vitro experiments.
- Fracture healing is a complex process involving multiple cells. The in vitro validation of this experiment focused only on the osteogenic differentiation of stem cells, and ignored the phenotypic transformation of other cells.
- The protein levels and functional research of the selected hub genes should be further validated.

Introduction

Most fractures can be repaired by spontaneously forming callus tissue with certain mechanical qualities, as long as the fracture site can retain contact.[1] There is evidence that delayed fracture healing, or nonunion, occurs in an estimated 5% to 10% of fractures.[2] Nonunion rates can reach up to 30% in people who have undergone plate fixation.[3] Nonunion of fractures not only poses a clinical challenge, but also results in a high burden on healthcare systems.[4,5]

The stiffness of the plate fixation structure can affect the fragment movement at the fracture site, which may cause stress shielding and affect the healing environment of the fracture.[6,7] A previous animal study has demonstrated that flexible fixation significantly promotes callus tissue formation and accelerates fracture healing.[8] One clinical study has found that fracture dynamization promotes callus formation, accelerating both the speed and strength of fracture healing.[9] For instance, Ren et al[10] compared the therapeutic outcomes of steel plates and elastic intramedullary nails in clavicle fractures and noted a shorter healing time in the elastic intramedullary nail fixation group. They introduced the concept of elastic osteosynthesis (EO), a technique that employs elastic fixation to maintain stress stimulation at the fracture site, thereby potentially promoting fracture healing. The healing of fractures is accompanied by interactions between cells and signalling molecules. The transmission of biological signals between cells and the coordination of gene function together constitute the fracture microenvironment. Osteoblasts and their precursor cells are sensitive to mechanical stimuli and have an ability to translate the mechanical signals into biological responses, such as an increase of cell viability, reorganization of the cytoskeleton, and secretion of extracellular matrix (ECM). Other studies have proven that mechanical stimulation can regulate osteoblast proliferation and differentiation by releasing signalling molecules within osteocytes, such as rapid changes in the intracellular calcium ion concentration, nitric oxide release, cytoskeleton reorganization, increased type II cyclooxygenase expression, prostaglandin release, and ECM synthesis.[11-13] In short, mechanical stress is an important parameter for fracture repair and healing because it effectively promotes callus formation and accelerates fracture healing.[14] Accurately understanding the signal transduction of these changes, especially the molecular mechanisms underlying phenotypic changes in cells stimulated by mechanical stress, is crucial for optimizing the fracture microenvironment and promoting fracture healing.

Scholars have begun to focus on maintaining a stress environment at the fracture site to improve healing. However, research on the molecular mechanisms of stress-promoting fracture healing is still insufficient. In clinical research, it is impossible to separate the callus tissue during healing. Rabbit bones are easy to observe, making them widely used in long-bone fracture models.[15] The purpose of this experiment was to: 1) study the mechanism of promoting fracture healing by elastic fixation through proteomics; and 2) explore the effects of stress stimulation on bone marrow mesenchymal stem cells (BMSCs) from the perspective of fracture microenvironment. We believe that that stress stimulation can affect fracture healing by modulating the fracture microenvironment. We also hypothesized that elastic fixation could promote callus tissue formation and fracture healing, and that callus tissue has a high mechanosensitive protein expression, which can promote osteogenic differentiation of BMSCs. The flowchart of this experiment is shown in Figure 1.

Methods

Four-point bending test

Intramedullary nail instruments with varying diameters of the Ti-6Al-4V (TC4) titanium alloy materials were chosen. Intramedullary nails with diameters of 1.5 mm and 3.0 mm were applied in the elastic and stiff fixation groups, respectively. The four-point bending test[16] is used to analyze the mechanical properties of different intramedullary nail instruments. The mechanical properties of the nails were determined using a four-point bending testing machine (CMT5504; Shenzhen Sansi Testing Equipment China). The nail was placed on two lower supports with a span length (L2) of 60 mm and an upper span length (L2) of 22 mm. Specimens were loaded to failure at a 0.5 mm/min rate, producing a force-displacement curve for each sample. The mechanical properties were directly obtained from these curves. The bending strength is the bending moment required to produce a 0.2% offset (plastic deformation) in the nails.[17] The four-point bending experiment revealed that the mean bending strength of 1.5 mm (0.32 N*m (SEM 0.05)) intramedullary nails was substantially lower than that of 3.0 mm (4.41 N*m (SEM 0.56)) intramedullary nails ($p < 0.001$, independent-samples *t*-test) (Figure 2).

Animal experiments

The reporting of animal experiments adhered to the ARRIVE guidelines, and an ARRIVE checklist is included in the Supplementary Material to show this.[18] For the experiments, 12-week-old male Japanese white rabbits (weight: 2 to 3 kg) were purchased from Beijing Huafukang Biotechnology (SCXK: 2020 0002; China), with one rabbit per cage kept in a well-lit environment free from pathogens. Next, 12 Japanese white rabbits were randomly divided into stiff fixation and elastic fixation groups (six rabbits each). Three rabbits were used for histological observation, and the remaining three were used for proteomic analysis in each group. Random numbers were generated using a computer-based random-order generator. A rabbit model of closed tibial fracture was established through three-point bending. The rabbits were anaesthetized with intramuscular injection of ketamine hydrochloride (40 mg/kg) and xylazine (5 mg/kg, 100 mg/ml) (Gutian Pharmaceutical Company, China) before the operation. Following the operation, rabbits were administered carprofen (2.2 mg/kg; Pfizer, USA) for postoperative analgesia for three days. Researchers monitored animals once a day to

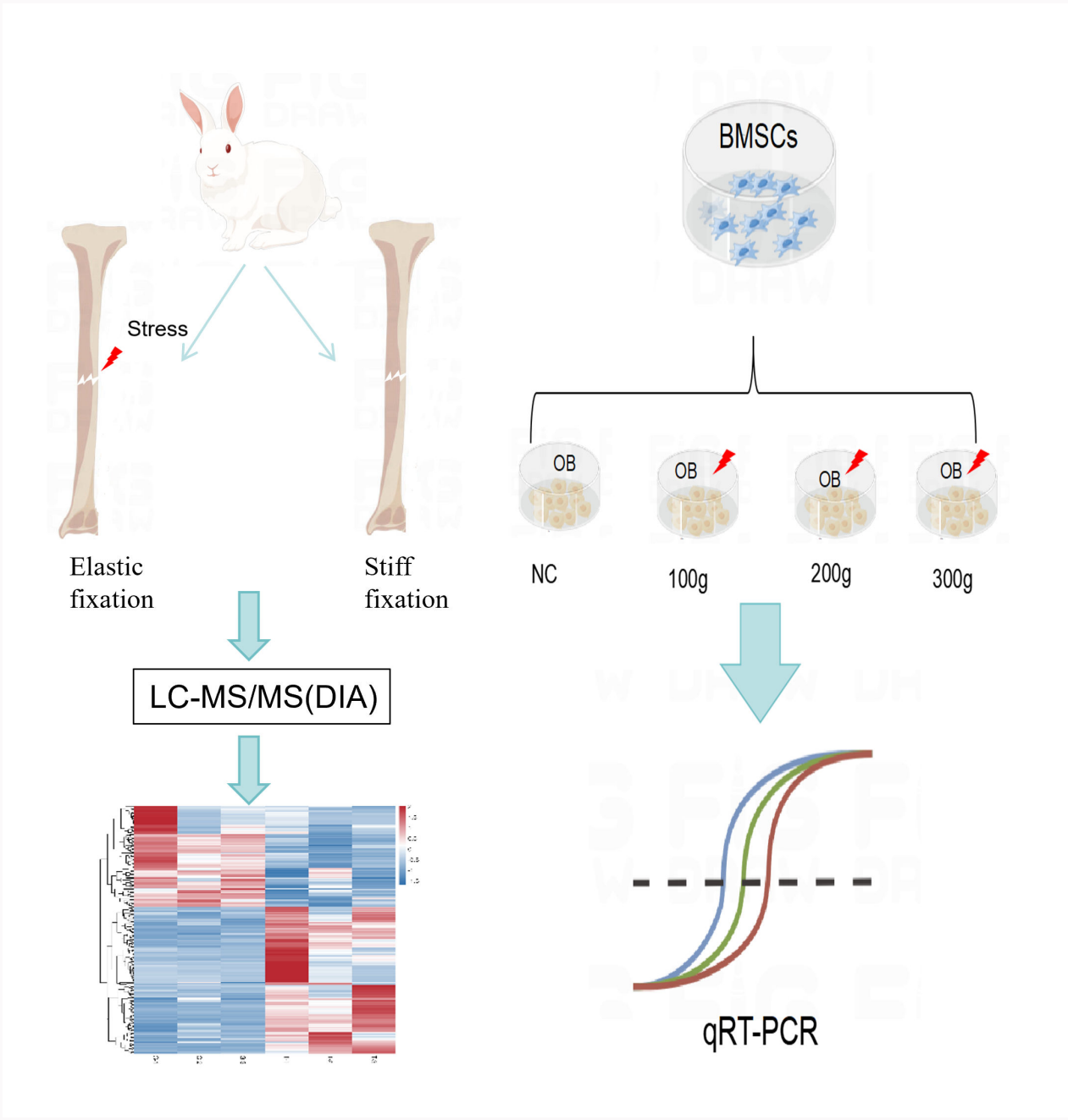

Fig. 1
The rabbits were divided into an elastic fixation group (preserve stress) and a stiff fixation group, and proteomic analysis was performed on the callus. Then, through in vitro experiments to simulate the stress environment of bone marrow mesenchymal stem cells (BMSCs) in callus, further screening of target genes was carried out. LC-MS/MS(DIA), liquid chromatography-mass spectrometry/mass spectrometry (data independent acquisition); NC, negative control; OB, osteoblasts; qRT-PCR, quantitative real-time polymerase chain reaction.

monitor their health status through weight, food, and water intake, and the general assessment of animal activity. The study included animals that had successfully established a fracture model and underwent intramedullary fixation surgery. Animals were excluded if they died prematurely, making it impossible to collect behavioural and histological data. During this experiment, one rabbit died due to side-effects of anaesthesia, and a new rabbit was added. The experimenters (ZZ, GZ) conducting animal operations and the experimenter (ML) conducting data analysis were different individuals to ensure that the data analysis personnel were blinded. Rabbits were raised two weeks after the operation and euthanized by excessive injection of anaesthesia with ketamine hydrochloride and xylazine.

Establishment of fracture model

After administering anaesthesia, intramedullary nails of different diameters were inserted into the medullary cavity of the tibia through the upper end of the tibia (1.5 mm diameter was used in the elastic fixation group, while a 3.0 mm diameter was used in the stiff fixation group). The closed fracture model production method employs a self-designed three-point bending fracture model apparatus, as illustrated in Figure 3. The procedure involves immobilizing the tibia

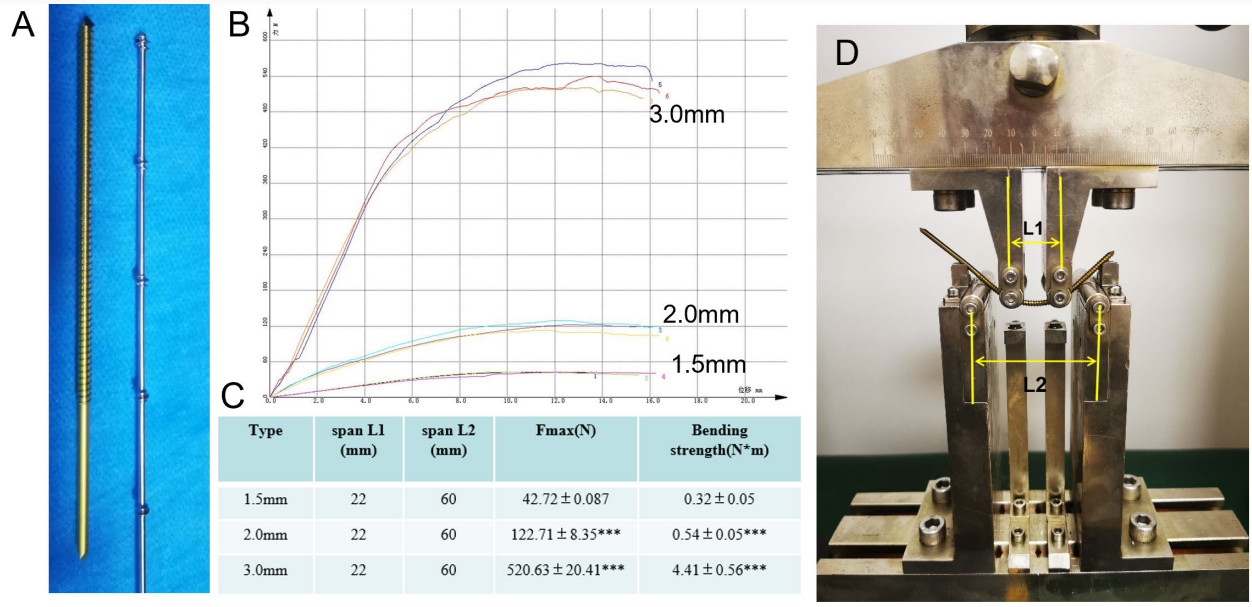

Type	span L1 (mm)	span L2 (mm)	Fmax(N)	Bending strength(N*m)
1.5mm	22	60	42.72 ± 0.087	0.32 ± 0.05
2.0mm	22	60	122.71 ± 8.35***	0.54 ± 0.05***
3.0mm	22	60	520.63 ± 20.41***	4.41 ± 0.56***

Fig. 2
Four-point bending test. a) The appearance of intramedullary nails. b) The force-displacement curve for each sample. c) Specific parameters of the four-point bending experiment. d) Four-point bending experiment for nails. ***T-test, $p < 0.001$ versus 1.5 mm. The mechanical experiment was independently repeated three times for the intramedullary nails representing different thicknesses.

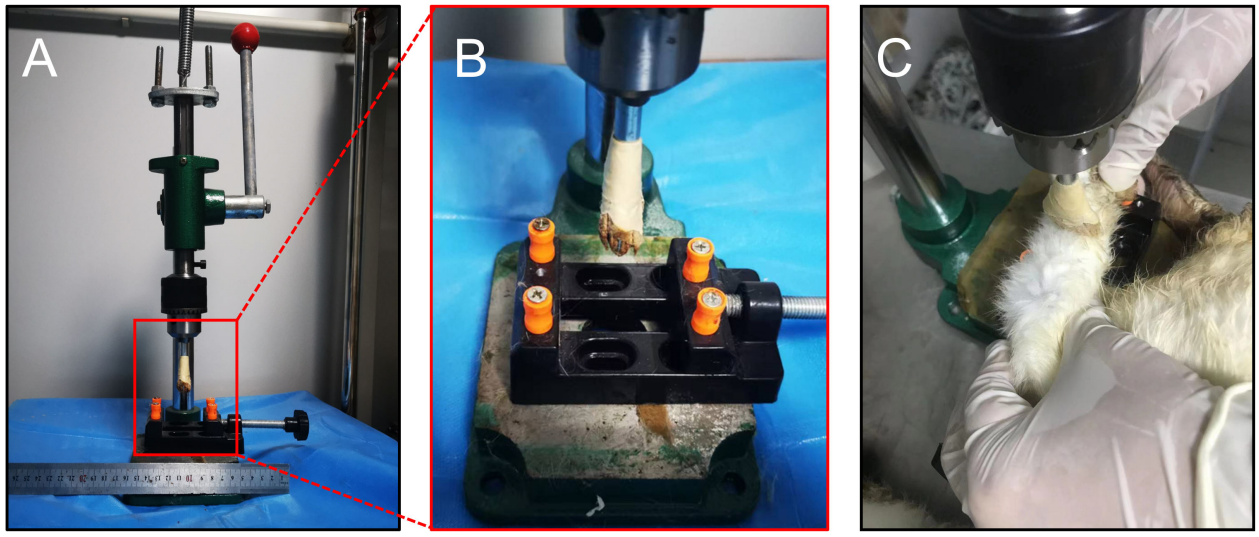

Fig. 3
Three-point bending fracture model apparatus. a) The appearance of fracture model apparatus. b) The lower groove of the fracture model apparatus. c) The usage process of fracture model apparatus.

of rabbits under anaesthesia within the fixed groove at the lower end of the apparatus. The horizontal span of the lower groove is adjusted based on the length of the rabbit's tibia, typically averaging 60 mm. Positioned above the groove is a manual stamping head, securely placed above the rabbit's tibia to ensure that the mechanical loading point aligned with the midpoint of the tibia. The assistant (GZ) assisted in securing the rabbit's tibia within the lower groove, while another manually applied downward pressure on the operating rod of the stamping machine, causing the stamping head to descend until it makes contact with the rabbit's tibia. Pressure continued to increase until the distinct sound of bone fracture was audible, indicating successful fracture creation. Subsequently, the pressure rod was lifted, followed by imaging examinations to confirm the model's successful establishment.

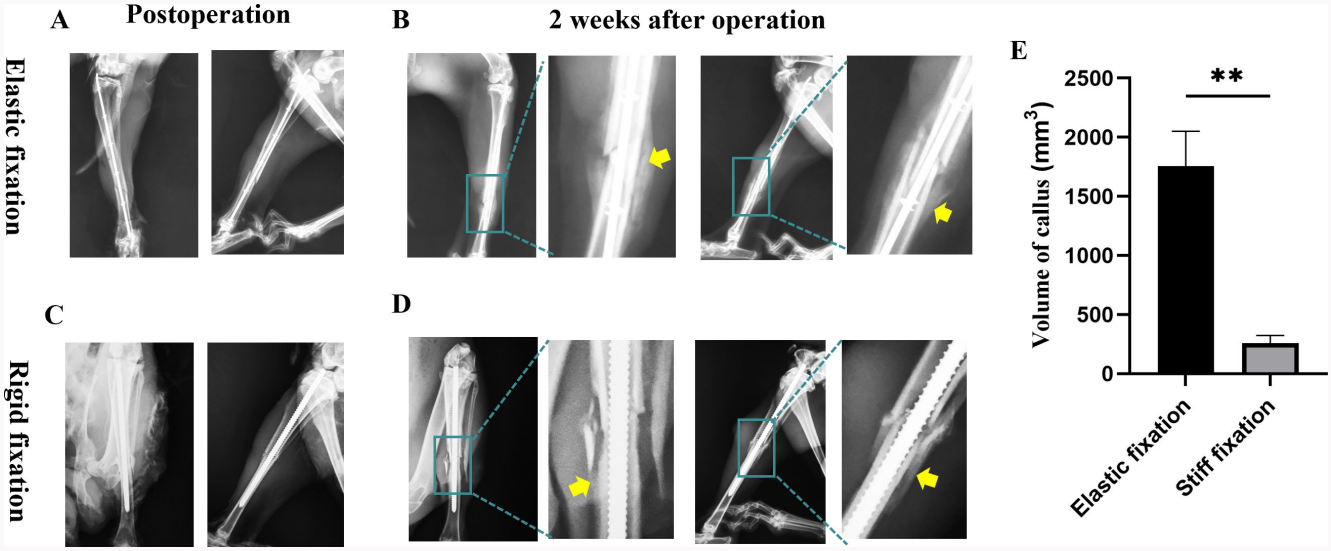

Fig. 4

Radiograph examination of different fixation methods for fractures. a) Closed reduction and elastic intramedullary fixation of tibial fractures. b) Radiograph examination after two weeks in the elastic fixation group. c) Closed reduction and stiff fixation of tibial fractures. d) Radiograph examination after two weeks in the stiff fixation group. e) Comparison of callus volume between two groups. **t-test, p 0.01 versus stiff fixation group. Each experiment was independently repeated three times. The yellow arrow represents the new callus formation.

Table I. Primer sequences used for the quantitative real-time polymerase chain reaction analysis.

Gene	Forward primer	Reverse primer
OSX	5′ -TTCGGATGAGCTGGAACGTC-3	5′ -TTTGCTCAGGTGGTCACTCC-3′
COL1α1	5′ -GCAAGAACGGAGATGACGGAGAAG-3′	5′ -ACCATCCAAACCACTGAAACCTCTG-3′
FN1	5′ -ATGCCTCCACTGCCATTGAT-3′	5′ -CCAGTTGGGGAAGCTCATCT-3′
OGN	5′ -ACCTTCGACTATGCAGCAGAT-3′	5′ -AGCAAGTGGGCATTTCATCAT-3′
LUM	5′ -CCTCCCCGCATCTCTTCTAAC-3′	5′ -AGAAGCTCTTCACTTCAAACTTTTC-3′
THBS1	5′ -AGTGTCGCTGTCAGAACTCAG-3′	5′ -GCAAGAGGTCCACTCAGACC-3′
COL12A1	5′ -AACGAGGTTTGCCAGGAGAG-3′	5′ -GGCACGTACGGCTCTGGATA-3′
GAPDH	5′ -GCCTGGAGAAAGCTGCTAAGT-3′	5′ -GAGTGGGTGGCACTGTTGAA-3′

COL12A1, collagen, type XII, alpha 1; COL1α1, collagen, type I, alpha 1; FN1, fibronectin 1; GAPDH, glyceraldehyde 3-phosphate dehydrogenase; LUM, lumican; OGN, osteoglycin; OSX, osterix; THBS1, thrombospondin 1.

Fracture healing assessment

Two weeks after the operation, three rabbits from each group were randomly selected. Radiograph examinations were performed to evaluate fracture healing and observe bone callus formation. The callus volume was measured using the Perkins method ($V = 2\pi r1 (r2–r1) L$, where r1 is the radius of the bone, r2 is the radius of the callus, and L is the length of the callus.[19] The callus volume was calculated and statistically compared.

Immunohistochemical staining

The callus specimens were decalcified with 10% ethylenediaminetetraacetic acid for 14 days. The callus samples were embedded in paraffin and sliced into 5 μm thick slices. Paraffin-embedded callus tissue sections were dewaxed in xylene, dehydrated in a graded alcohol series, and subjected to antigen retrieval in proteinase K for 15 minutes at 37°C. Next, the slices were blocked with 5% bovine serum albumin (BSA) for 30 minutes, incubated with the corresponding primary antibodies (osterix (OSX) (1110 R) and collagen, type I, alpha 1 (COL1α1) (0578 R; both Bioss, China)) at 4°C overnight (negative control (NC): the first antibody is replaced by phosphate-buffered saline (PBS), and incubated with a horseradish peroxidase-conjugated secondary antibody (1:1,000; Beyotime, China) at room temperature for two hours. Finally, colour reactions were performed using a diaminobenzidine (DAB) peroxidase substrate (Vector Laboratories, USA) after treating sections with a mixture of avidin and biotinylated horseradish peroxidase. The stained images were photographed using a light microscope (Thermo Fisher Scientific, USA) and analyzed using Image-Pro Plus software (Media Cybernetics, USA).

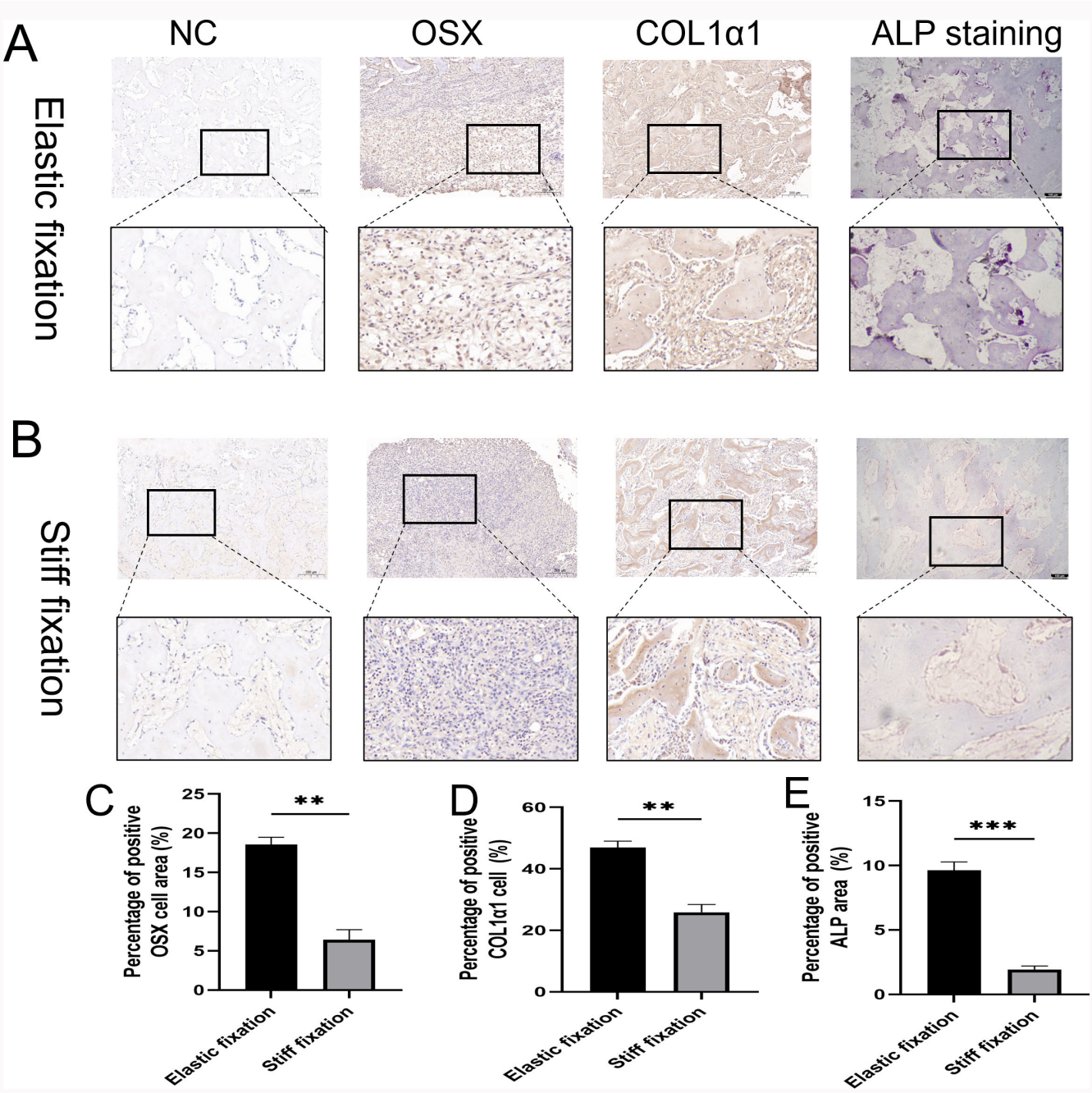

Fig. 5

Pathological examination of callus tissue. Osterix (OSX), collagen, type I, alpha 1 (COL1α1) immunohistochemistry staining (DAB staining, magnification factor 100×, scale bar = 200 μM), and alkaline phosphatase (ALP) staining (DAB staining, magnification factor 50×, scale bar = 100 μM) in a) the elastic fixation group and b) the stiff fixation group. c) to e) Quantitative analysis of OSX, COL1α1, and ALP. t-test, *p < 0.05, **p < 0.01, ***p < 0.001 versus the stiff fixation group, Each experiment was independently repeated three times.

Data-independent acquisition proteomics

The callus tissue was separated and preserved. Briefly, 30 μl of solvent A (A: 0.1% formic acid aqueous solution) was added to each sample to make a suspension, 9 μl was taken, and 1 μl 10× IRT peptide was added, mixed, separated with nanoflow liquid chromatography (nano- LC), and analyzed using online electrospray tandem mass spectrometry. The entire experimental system was an Orbitrap Fusion Lumis mass spectrometer (Thermo Fisher Scientific, USA) connected in series with an EASY-nLC 1200 system (LC140, Thermo Fisher Scientific). Three samples (Analytical Column Accum PepMap C18, 75 μM × 25 cm) were separated with 120 min-gradient : from 5% to 35% B (B: 0.1% formic acid acetonitrile (ACN) solution) within 120 minutes. The column flow was controlled at 200 nl/min, and the electric spray voltage was 2 kV. The mass spectrometry parameters were set as follows: 1) MS: scanning range (m/z): 350 to 1,500; resolution: 120,000 full width at half maxima (FWHM); automatic gain control (AGC) target: 4e6; maximum injection time: 50 ms; 2) host cell DNA mass spectrometry/mass spectrometry (HCD-MS/MS): resolution, 30,000; AGC target, 1e6; collision energy, 32 eV; energy increase, 5%; 3) variable window acquisition, with 60 window sets and overlapping serial port sets, with each window overlapping by 1 m/z; and 4) Log2 fold change

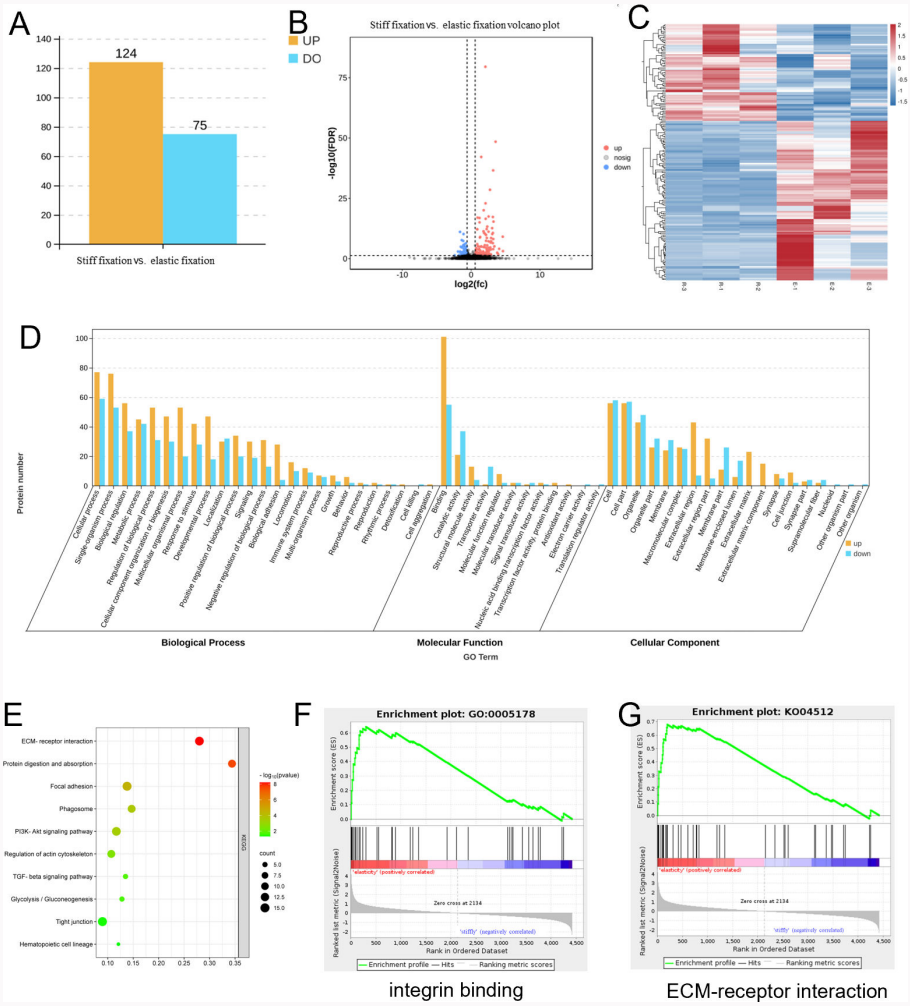

Fig. 6

Comparison of the protein expression of elastic fixation and stiff fixation. a) A number of proteins with different fixation methods ($p < 0.05$, fold change ≥ 1.5, independent-samples *t*-test). b) Volcano maps of proteins with different fixation methods. c) Heatmap of differentially expressed proteins (DEPs) that are associated with elastic fixation and stiff fixation. d) and e) Gene Ontology (GO) and Kyoto Encyclopedia of Genes and Genomes (KEGG) enrichment analyses of differential proteins (p 0.05, hypergeometric test). f) and g) Gene Set Enrichment Analysis (GSEAof differential proteins Each experiment was independently repeated three times. DO, downregulated; ECM, extracellular matrix; nosig, no significant difference; TGF, transforming growth factor; UP, upregulated.

(Log2FC) value thresholds were chosen as ≥ 1.5 or ≤ 1.5 with adjusted p-value < 0.05 (Benjamini-Hochberg method).

Protein-protein interaction networks

Differentially expressed proteins (DEPs) were introduced into the STRING functional protein association network (version: 19.0; University of Zurich, Switzerland) for protein interaction,[20] and *Oryctolagus cuniculus* was selected with a medium confidence of 0.400. Furthermore, the protein-protein interaction (PPI) network modules were identified using the CytoScape software (University of California, San Diego, USA).[21] Significant modules were identified with Molecular COmplex DEtection (MCODE) score > 5. Then, CytoHubba (University of California, San Diego) was used to select the top ten hub genes based on the maximal clique centrality (MCC) algorithm.

Isolation and culture of bone marrow mesenchymal stem cells

Four Japanese white rabbits (0.75 kg, male, aged two to four weeks) were selected for this experiment. After intraperitoneal injection of 2% pentobarbital sodium (30 mg/kg), the skin and muscle layers of the legs were cut open, the tibia, femur, and soft-tissue were removed, the bone ends were cut, and the medullary cavity was exposed. The samples were rinsed with PBS containing 1% penicillin-streptomycin, filtered through a 200-mesh filter, and centrifuged at 500× g for ten minutes. The cells were resuspended in Minimum Essential Medium α (MEM-α) (32571036; Gibco, Thermo Fisher Scientific, USA) containing 10% fetal bovine serum, and cultured at 37°C and 5% CO_2. The medium was changed for the first time after 24 hours and then every 48 hours. The cell morphology and growth status were observed under a microscope (DM IL LED; Leica, Germany). After the cell growth and fusion reached 90%, the cells were inoculated and subcultured in a 1:2 ratio. This time, it was recorded as the first generation (P1). When transferred to the third generation (P3), the purity of mesenchymal stem cells was relatively high, and their morphology was stable. These cells were selected for subsequent experiments.

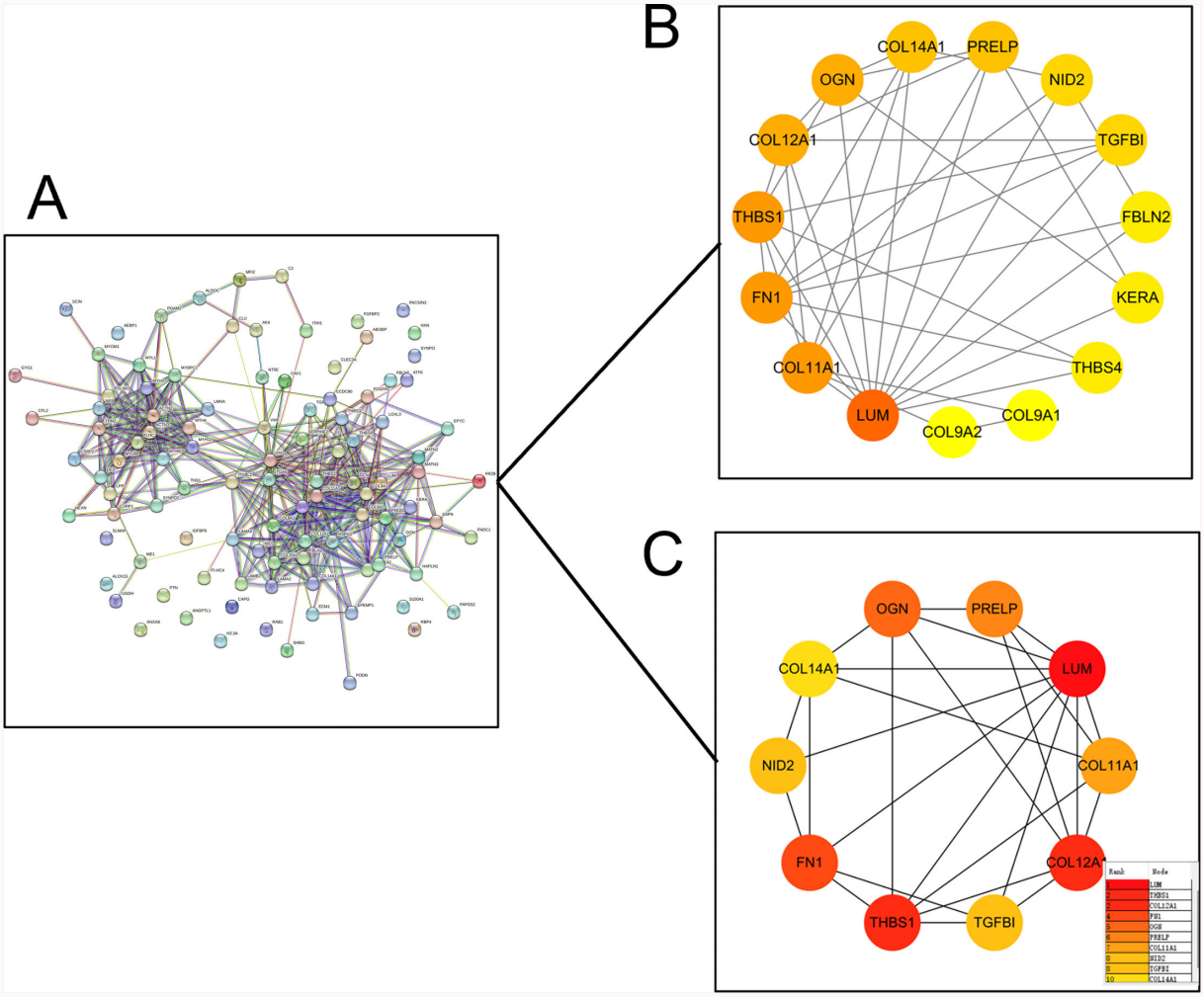

Fig. 7
Modules identified from the protein-protein interaction (PPI) network. a) PPI network showing the clusters of proteins with medium confidence (0.40) of interaction. b) The modules were identified using Molecular COmplex DEtection (MCODE) in Cytoscape, when 'MCODE score > 5' was defined as the cutoff criterion. c) CytoHubba plug-ins of the Cytoscape software were used to choose the top ten targets of maximal clique centrality (MCC).

Cellular mechanical stimulation

The force application method used in this experiment was based on the method proposed by Fitzgerald and Hughes-Fulford.[22] Mesenchymal stem cells were mechanically loaded using a centrifuge (Allegra X-30R; Beckman Coulter, USA). BMSCs were arbitrarily divided into four groups, all being seeded simultaneously. The NC group received no mechanical force loading, while the 100, 200, and 300 g groups received 100, 200, and 300 g stress stimulation for 30 minutes/day, respectively. On the day before stress stimulation, the culture medium was replaced with an osteogenic induction medium (Cyagen Biosciences, USA).

Alizarin red staining and calcium content detection

BMSCs were inoculated into a six-well plate and replaced with an osteoblast induction medium (GUXMX-90021; Cytogen, USA). Alizarin red staining and quantitative testing were performed for each group at fixed timepoints after 14 days of force application. The cells were fixed with 70% ethanol. After 30 minutes, the cells were rinsed three times with double-distilled water. Briefly, 500 µl of Alizarin red staining solution (C0148S; Beyotime) was added to each well for staining. The cells were left to stand at room temperature in the dark for 15 minutes. After draining the staining solution, the cells were washed three times with double-distilled water. The staining was observed under an inverted microscope (DM IL LED, Leica, Germany). Then, 500 µl of 10% cetylpyridine chloride was pipetted and incubated in each well for 30 minutes. Next, 200 µl of the sample was taken from each well and added to a 96-well plate. The wavelength of the light wave was set to 562 nm using a microplate spectrophotometer (Thermo Fisher Scientific), and the absorbance value of the sample was measured.

Alkaline phosphatase staining

Alkaline phosphatase (ALP) staining was conducted using a tartrate-resistant acid phosphatase (TRAP)/ALP double staining kit (294-67001; Wako Pure Chemical Industries, Japan). For paraffin section staining, 0.5 ml of ALP staining solution was added to each section at room temperature within a wet chamber and left for 30 minutes. The colour development time varied based on the ALP amount and activity in the samples. Once the appropriate reaction state was observed under the microscope (DM1000, Leica), it was halted. The slices were soaked in distilled water for three minutes, dried on a heating plate at 37°C, and sealed with

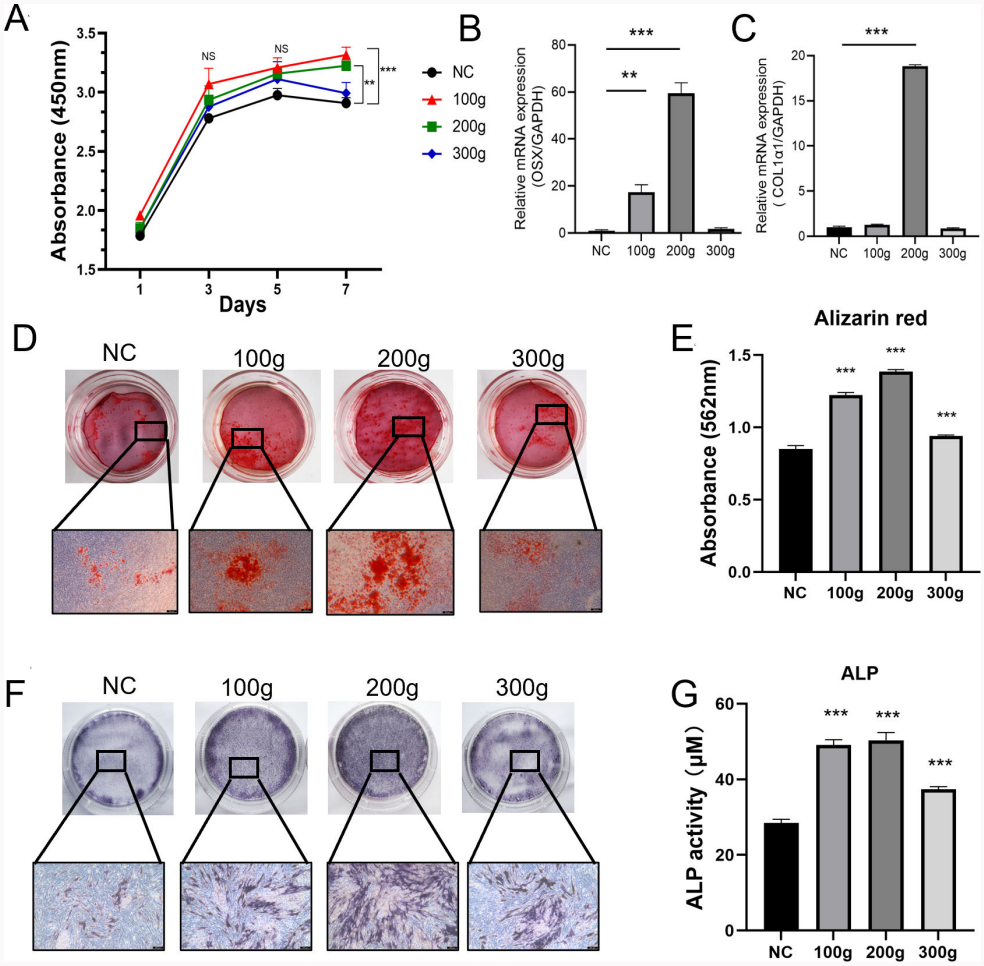

Fig. 8

Mechanical stimulation culture of bone marrow mesenchymal stem cells (BMSCs). a) Cell viability of BMSCs cultured under different stress sizes. b) and c) Messenger RNA (mRNA) expression of osterix (OSX) and collagen, type I, alpha 1 (COL1α1) in BMSCs after seven days of different stress sizes. d) and e) Alizarin red staining and semi-quantitative analysis of calcified nodules in BMSCs after 21 days of stress of different sizes (magnification factor of histology image 50×). f) and g) Alkaline phosphatase (ALP) staining and semi-quantitative analysis in BMSCs after ten days of stress at different sizes (magnification factor of histology image 50×). *p < 0.05, **p < 0.01, ***p < 0.001 (analysis of variance) versus negative control (NC) group. Each experiment was independently repeated three times. GAPDH, glyceraldehyde 3-phosphate dehydrogenase.

a sealing agent for observation. For cell staining, after cleaning the cells with PBS, 500 μl of pre-cooled 4% paraformaldehyde was added and kept on ice for ten minutes for cell fixation. The remaining fixative was washed with PBS, and 500 μl of ethanol/acetone (50:50 v/v) solution was added and incubated at approximately -30°C to -20°C for one minute. Next, 2 ml of PBS was added, and this step was repeated twice. Then, 250 μl of ALP substrate was added to each well. It was covered with a porous plate to prevent drying and allowed to react for 30 minutes at 37°C.

Alkaline phosphatase content detection

An ALP detection kit (P0321S; Beyotime, China) was used to detect the ALP content. The samples were prepared and washed three times with PBS. The cells were lysed with 1% Triton X-100 for 30 minutes, the supernatant was centrifuged (12,000 rpm for 15 mins), and 50 μl of the sample was added to 96-well plates. Then, 50 μl of chromogenic substrate was added, mixed, and incubated at 37°C for 30 minutes. Next, 100 μl of reaction termination solution was added to each well to terminate the reaction. Absorbance was measured at a wavelength of 405 nm. The ALP activity was calculated in the sample based on the definition of enzyme activity.

Cell counting kit-8 assay

The BMSCs were diluted to 5 × 10^4 cells/ml density. Then, 100 μl of cell solution was transferred to each well of a 96-well plate and incubated overnight at 37°C to allow BMSCs to adhere to the wall. After one, three, five, and seven days of mechanical loading, CCK-8 (CA1210; Solarbio, China) was diluted with a complete culture medium at a ratio of 10:1. Then, 100 μl of the diluted solution was transferred to the BMSC in each well. After co-incubation for two hours, a microplate spectrophotometer (Multiskan, Thermo Fisher Scientific) was used to measure absorbance at 450 nm.

Quantitative real-time polymerase chain reaction

Quantitative real-time polymerase chain reaction (qRT-PCR) was performed using the Cobas z 480 detection system (Roche, Switzerland) and the SYBR PrimeScript RT-PCR kit (Takara Bio, Japan). The primer sequences used are listed in Table I. The PCR system consisted of the following components: SYBR Green 10 μl, upstream and downstream

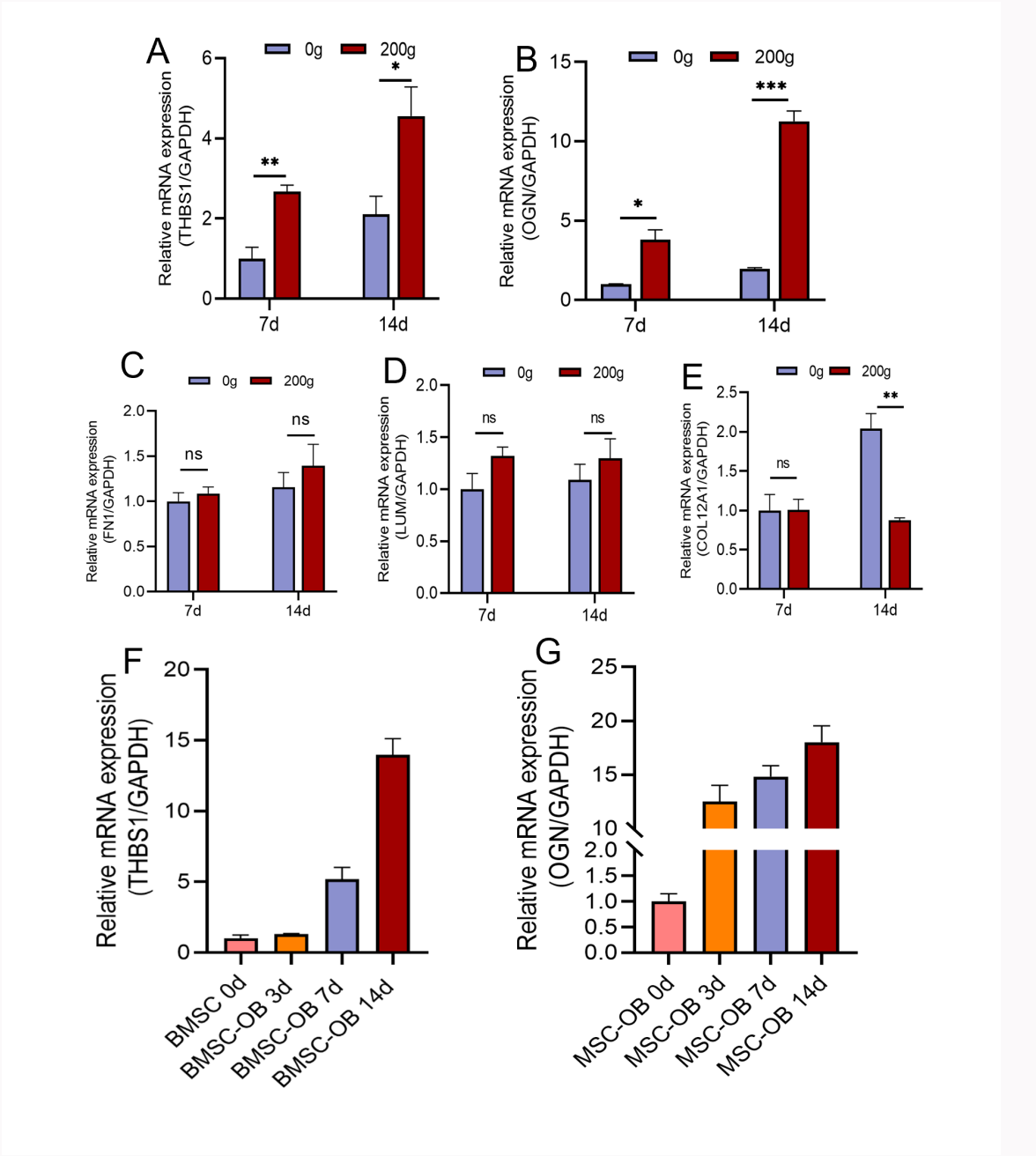

Fig. 9

Further screening of hub genes. a) to e) Effects of 200 g stress stimulation on messenger RNA (mRNA) expression of hub genes thrombospondin 1 (THBS1), osteoglycin (OGN), fibronectin1 (FN1), lumican (LUM), and collagen, type XII, alpha 1 (COL12A1) on days 7 and 14. f) and g) Relative mRNA expression of THBS1 and OGN in bone marrow mesenchymal stem cell (BMSC) induced osteoblasts (OB) on days 0, 3, 7, and 14. *p < 0.05, **p < 0.01, ***p < 0.001 (ANOVA) versus the negative control (NC) group. Each experiment was independently repeated three times.

primers 0.5 μl each, enzyme-free water 7.0 μl, and cDNA 2.0 μl, with a total volume of 20 μl. The PCR reaction conditions were 95°C for one minute, followed by 40 cycles at 95°C for 15 seconds, 60°C for 45 seconds, and 72°C for 15 seconds. The relative expression level of the target gene was calculated using the cyclic Ct values obtained from the PCR detection software and the formula 2^{-} Ct, with glyceraldehyde 3-phosphate dehydrogenase (GAPDH) as the internal reference gene.

Statistical analysis

GraphPad Prism (version 9.0; GraphPad Software, USA) was used for statistical analyses. All experimental data were presented as the mean and standard error of the mean (SEM). The comparison between two groups was conducted using independent-samples *t*-test, and the comparison between multiple groups was conducted using analysis of variance (ANOVA). One-way analysis of variance was used if the data in each group followed a normal or approximately normal distribution and the variances between groups were uniform. Wilcoxon signed-rank test/Mann-Whitney U test or Kruskal-Wallis test was used if the data did not conform

to the normal distribution. Tukey's test was used for post-hoc multiple comparisons to identify statistically significant differences between groups. Hypergeometric test was used for Gene Ontology (GO) and Kyoto Encyclopedia of Genes and Genomes (KEGG) enrichment analyses, and $p < 0.05$ was considered statistically significant.

Results

Elastic fixation promotes fracture healing

Two weeks after the operation, radiographs revealed that the elastic fixation group had greater callus formation than the stiff fixation group (Figure 4). After measuring the callus volume using the Perkins method, the mean callus volume was larger in the elastic fixation group (1,755 mm^3 (SEM 297)) than in the stiff fixation group (258 mm^3 (SEM 65)), with a statistically significant difference (t-test, $p = 0.008$). The mean percentage of positive OSX cells in the callus tissue was higher in the elastic fixation group (46.94% (SEM 2.10)) than in the stiff fixation group (25.85% (SEM 2.59); t-test, $p = 0.003$). Simultaneously, the elastic fixation group showed markedly improved mean positive COL1α1 area (6.43% (SEM 0.01) vs 18.55% (SEM 0.01); $p = 0.001$) and increased mean ALP expression (1.94% (SEM 0.01) vs 9.63% (SEM 0.01); both t-test, $p = 0.003$) in the callus group compared with the stiff fixation group (Figure 5).

Proteomic analysis of callus tissue

We identified 199 DEPs, 124 upregulated in the elastic fixation group using proteomic analysis (t-test < 0.05; fold change > 1.5;). (GO) terms, representing specific concepts in the GO hierarchy, play a crucial role in annotating genes and analyzing their functional characteristics. In this study, significantly enriched terms in biological process (BP), molecular function (MF), and cellular component (CC) categories were selected. DEPs are primarily involved in cellular processes, binding, and biological regulation. (KEGG) pathway enrichment analysis showed that DEPs were mainly involved in ECM-receptor interaction, the PI3K-Akt signalling pathway, and the transforming growth factor beta (TGF-β) signalling pathway . Gene Set Enrichment Analysis (GSEA) revealed that proteins upregulated in the elastic fixation group are enriched in the ECM-receptor interaction and integrin binding.(Figure 6)

Next, a PPI network was constructed using the STRING database to better understand the DEPs (Figure 7a). Then, the plugins MCODE and CytoHubba were used to select the core targets (Figure 7c). The top five core targets were lumican (LUM), thrombospondin 1 (THBS1), collagen, type XII, alpha 1 (COL12A1), fibronectin1 (FN1), and osteoglycin (OGN).

Cellular mechanical stimulation

BMSCs were subjected to mechanical stimulation and divided into four groups based on the magnitude of the mechanical stress. The CCK-8 results showed that after seven days of BMSC cultivation, the mean absorbance values of the 100 (3.32 (SEM 0.67)) and 200 g (3.22 (SEM 0.04)) groups were significantly increased compared with the NC group (2.91 (SEM 0.04); t-test, $p = 0.03$), indicating that stress stimulation of 100 to 200 g can enhance the proliferation ability of BMSCs (Figure 8a). The qRT-PCR results showed that after seven days of cell culture with force, the loading condition of 200 g force significantly increased the osteogenic-related genes OSX and Col1α1 compared with the NC group ($p = 0.001$, ANOVA; Figure 8c). After 14 days of osteogenic induction, Alizarin red staining was performed. The results showed that the number of mineralized nodules formed was significantly increased in each force group compared with the NC group (Figure 8d). Calcium content measurement showed that the mean calcium content significantly increased in the 100 (1.22 (SEM 0.01)), 200 (1.38 (SEM 0.01)), and 300 g groups (0.94 (SEM 0.01)) compared with the NC group (0.85 (SEM 0.01)). The 200 g booster group showed the most significant increase ($p < 0.001$, ANOVA; Figure 8e). The ALP activity measurement results showed that the mean ALP activity of the 100 (49.09 μM (SEM 0.79)), 200 (50.33 μM (SEM 1.19)), and 300 g groups (37.36 μM (SEM 0.41)) was significantly increased compared with the control group (28.48 (SEM 0.54)) at Day 14 ($p < 0.001$, ANOVA; Figure 8g).

In summary, a certain level of mechanical stress stimulation can promote the osteogenic differentiation of BMSCs, with the 200 g stress group being the most significant. Therefore, 200 g of stress-cultured BMSCs were used in the subsequent experiment. qPCR results showed that in BMSCs cultured under stress for seven days, the mean mRNA expression of THBS1 (1 (SEM 0.28) vs 2.67 (SEM 0.16)) and OGN (1 (SEM 0.02) vs 3.80 (SEM 0.61)) was significantly greater in the 200 g group than in the NC group ($p < 0.001$, ANOVA). After 14 days of cultivation, the mRNA expression of THBS1 (2.10 (SEM 0.45) vs 4.55 (SEM 0.73)) and OGN (1.95 (SEM 0.08) vs 11.26 (SEM 0.65)) was significantly greater in the 200 g group than in the control group ($p = 0.002$, ANOVA). The mRNA expression of THBS1 and OGN increased progressively during osteogenic induction, indicating that THBS1 and OGN contributed to osteoblast differentiation (Figure 9).

Discussion

Previous research has shown that the local mechanical environment at the fracture site plays an important regulatory role in fracture healing, and retaining the stress environment at the fracture site can accelerate the healing speed of fractures.[23] Over the past 20 years, there has been a growing body of evidence indicating that the mechanical stresses exerted by cells and tissues, as well as the physico-chemical characteristics of the cell microenvironment, are crucial in regulating both physiological and pathological conditions. In both contexts, cells are compelled to adjust their activities through the conversion of physical cues into biochemical signals and alterations in gene expression via mechano-chemical transduction or mechanotransduction pathways.[24] Presently, it is evident that a comprehensive correlation exists between the physicochemical characteristics of the microenvironment and gene expression. Mechanobiology has served as the foundation for numerous scientific breakthroughs in elucidating how biophysical and biomechanical cues control cell behaviour.[25] However, more investigation is required to determine how mechanical stimulation affects fracture healing by regulating the fracture microenvironment. This study uncovered the underlying biological mechanism of the biomechanical environment promoting fracture healing using animal and proteomic technology.

A rabbit fracture heals three times faster than a human fracture, and can be repaired in four weeks.[26,27] Therefore, we used rabbits as the research subjects. After a fracture occurs, it undergoes an inflammatory phase (one week), during which

BMSCs begin to migrate to the fracture site. Then, it enters the phase of callus formation (two to three weeks). On one hand, the BMSCs around the periosteum near the fracture site begin to transform into osteoblasts, a process named intramembrane ossification. On the other hand, fibrous tissue in the fracture site transforms into cartilage, and chondrocytes gradually undergo apoptosis and are replaced by osteoblasts differentiated from BMSCs, a process named endochondral ossification. Finally, the fracture enters the callus-shaping phase (four weeks), where osteoclasts differentiate and shape the formed callus.[28] Callus formation occurs approximately two weeks after the fracture is sustained, and is the most active period for osteoblast differentiation. Therefore, we selected callus for research during this period. Pathological observation revealed that elastic fixation significantly increased osteoblast marker protein expression in callus tissue, indicating that elastic fixation can promote osteoblast differentiation in callus tissue. We believe that the bending strength of the intramedullary nail in the elastic fixation group is lower, and micromovement occurs at the fracture site, which generates mechanical stimulation around the BMSCs at the fracture site, thereby promoting its osteogenic differentiation. Throughout the process, the callus can perceive the local mechanical environment and respond to it. These biomechanical signals are transmitted to cells to regulate gene expression, thereby regulating the fracture microenvironment.

According to proteomics research, 124 genes were highly expressed in the elastic fixation group. The proteomics results originated from the stage of callus formation, during which osteoblasts differentiate most actively. We also identified the hub proteins involved in this process among the DEPs. The vitality and differentiation ability of BMSCs gradually decreases with donor age.[29] We selected two- to four-week-old rabbits as cell donors for subsequent in vitro experiments. This study assumed that the mechanical environment at the fracture site could regulate the high protein expression, thereby promoting osteoblast differentiation. The micromovements in the fracture site decompose forces into various directional components due to the irregular geometrical shape of human bones in biomechanics, and the cells at the fracture site are exposed to a complex stress environment.[30] Therefore, this study simulated the in vivo differentiation environment of stem cells after two weeks of fracture healing, by culturing BMSCs in vitro and providing a mechanical environment through centrifugation.[22] First, the study compared centrifugal force with other forces and found that these different mechanical stresses cause similar changes in gene expression in cells, proving that centrifugation is an effective method for providing a stress environment for cells.[31] Additionally, centrifugal force does not need gel culture medium, meaning that the force can be directly loaded onto the cell, which can better simulate the cell's mechanical environment. Centrifugal force is easy to operate and has high repeatability, and is frequently used to simulate the effect of stress stimulation on extracellular proteins secreted by osteoblasts in vivo.[32]

In vitro validation revealed that mechanical stress stimulation of BMSCs could promote osteogenic differentiation. After stimulating BMSCs, the mRNA of THBS1 and OGN were upregulated. The THBS1 and OGN expressions gradually increased during osteoblast differentiation. This indicates that a specific level of mechanical stress stimulation can promote the osteogenic differentiation of stem cells by upregulating genes, such as THBS1 and OGN. Shi et al[33] found that THBS1 can promote osteogenic differentiation of MC3T3-E1 cells and upregulate the protein expression levels of ALP and COL1α1. Chen et al[34] found that BMSCs forced to express OGN with lentivirus increased the expression of ALP and COL1α1. When subjected to mechanical stimulation, cytoskeletal proteins undergo structural reorganization, converting mechanical signals into biological signals.[12] Filamin C (FLNC), an upstream protein among the cytoskeletal proteins, can regulate downstream cytoskeletal proteins and is highly expressed in the elastic fixation group.[35] We speculate that mechanical signals may activate the expression of FLNC, leading to BMSCs secreting more ECM proteins. However, this study focused on identifying proteins that promote bone differentiation, and we plan to improve the research on signal transduction pathways in future experiments. Mechanical stimulation of osteoblast lineage cells can increase integrin, ECM protein, and growth factor production, promoting osteogenic differentiation in an integrin-ECM-dependent manner.[36] Therefore, we believe that BMSCs, when stimulated by stress, activate the autocrine system to secrete more ECM proteins that can bind to integrin and regulate the intracellular osteogenic signalling pathway, thereby controlling stem cell proliferation and osteogenic differentiation.

Fracture healing is achieved by combining intramembrane and endochondral osteogenesis. Wong et al[37] found that mechanical stimulation caused by unstable fractures could induce chondrocytes to osteoblast transformation, thereby promoting endochondral ossification. The TGF-β pathway indicates a more cartilaginous callus in the elastic group. The TGF-β signalling pathway plays a key role in cartilage formation. After a fracture, TGF-β levels increase during endochondral ossification, which is helpful for callus formation.[38] Angiogenesis is a crucial component of fracture healing. After soft callus formation, blood vessels invade the calcified cartilage. The blood vessels invading the callus can recruit BMSCs and provide oxygen and nutrients to metabolically active regenerated callus tissues, promoting callus ossification. A recent study has confirmed that the PI3K/AKT signalling pathway is crucial in angiogenesis and enhances communication between bone cells.[39] Another study found that blood flow increased fourfold over two weeks in the elastic group.[40] The study observed the vessel volume and vessel diameter of neovascularization using vascular imaging technology, and found that performing micromovements at the fracture site may improve vascular formation at the fracture site.[41]

This study restricted the axial movement of the fracture site via threads, while elastic fixation allowed for lateral movement of the fracture site. This suggests a new idea that the shear motion may promote fracture healing. However, this requires stronger restrictions on the direction of the force acting on the fractured end. In their 1998 study, Park et al[27] discovered that axial shear motion could promote fracture healing. However, in 2010 Epari et al[42] argued in their study that the oblique osteotomy resulted in obvious compression, making it impossible to study the effects of pure shear. This experiment excluded comparing more flexible movements at the fracture site, because only the optimal strain could

accelerate fracture healing. When the applied micromotion exceeded 30% strain, it delayed union and nonunion.[43] This is consistent with our in vitro research results. Appropriate range of stresses can enhance the vitality and differentiation ability of BMSCs, and exceeding this range may lead to a decrease in osteogenic differentiation. Unlike in humans, the stress response of rabbits can lead to a wider range of motion for fractures, and more flexible fixation methods often result in obstacles to fracture healing.[44]

The reason why we excluded female animals is that there is an obvious difference in oestrogen levels between different female rabbits.[45] Maintaining consistent oestrogen levels within each group of rabbits is crucial to prevent potential interference with the comparative analysis of results across groups. Nevertheless, at an individual level, elastic fixation has been shown to enhance fracture healing irrespective of the rabbit's sex. This is attributed to the fundamental mechanism of elastic fixation, which triggers the differentiation of BMSCs at the fracture site in response to stress. Mechanical stimuli, rather than oestrogen levels, play a key role in promoting the osteogenic differentiation of BMSCs.

There are some limitations in this study. First, the healing process of fractures requires the involvement of multiple cells, including bone marrow mesenchymal stem cells, osteoblasts, chondrocytes, and osteoclasts. However, this study only focused on the role of the target gene in mesenchymal stem cells and ignored the role of the target gene in other cells. Second, in vitro experiments only validated the target gene at the gene expression level using qPCR, without verifying the expression changes of the target gene at the protein level.

In conclusion, in the process of fracture treatment, elastic fixation can create a favourable fracture microenvironment for fracture healing, thereby promoting fracture healing. A suitable mechanical environment can regulate the microenvironment of fracture. From a molecular biology perspective, appropriate mechanical stimulation provided a favourable biophysical environment for osteogenic differentiation of BMSCs, and the mechanism of mechanical stimulation promoting osteogenic differentiation of BMSCs may be achieved by upregulating THBS1 and OGN in BMSCs.

Supplementary material

An ARRIVE checklist is included to show that the ARRIVE guidelines were adhered to in this study.

References

1. **Zura R**, **Xiong Z**, **Einhorn T**, **et al**. Epidemiology of fracture nonunion in 18 human bones. *JAMA Surg*. 2016;151(11):e162775.
2. **Mangum LH**, **Avila JJ**, **Hurtgen BJ**, **Lofgren AL**, **Wenke JC**. Burn and thoracic trauma alters fracture healing, systemic inflammation, and leukocyte kinetics in a rat model of polytrauma. *J Orthop Surg Res*. 2019;14(1):58.
3. **Simpson AHRW**, **Tsang STJ**. Non-union after plate fixation. *Injury*. 2018;49 Suppl 1:S78–S82.
4. **Stewart CC**, **O'Hara NN**, **Bzovsky S**, **et al**. Bone turnover markers as surrogates of fracture healing after intramedullary fixation of tibia and femur fractures. *Bone Joint Res*. 2022;11(4):239–250.
5. **Dietrich G**, **Terrier A**, **Favre M**, **et al**. Influence of smoking on the healing of conservatively treated displaced midshaft clavicle fractures. *Bone Joint J*. 2023;105-B(7):801–807.
6. **Sainio H**, **Rämö L**, **Reito A**, **Silvasti-Lundell M**, **Lindahl J**. Prediction of fracture nonunion leading to secondary surgery in patients with distal femur fractures. *Bone Jt Open*. 2023;4(8):584–593.
7. **Giannicola G**, **Amura A**, **Sessa P**, **Prigent S**, **Cinotti G**. Assessment of progression and clinical relevance of stress-shielding around press-fit radial head arthroplasty. *Bone Joint J*. 2023;105-B(8):905–911.
8. **Claes L**, **Augat P**, **Suger G**, **Wilke HJ**. Influence of size and stability of the osteotomy gap on the success of fracture healing. *J Orthop Res*. 1997;15(4):577–584.
9. **Hu M**, **Zeng W**, **Zhang J**, **et al**. Fixators dynamization for delayed union and non-union of femur and tibial fractures: a review of techniques, timing and influence factors. *J Orthop Surg Res*. 2023;18(1):577.
10. **Ren L**, **Yang Z**, **Wang Y**, **et al**. Comparison of minimally invasive fixation of mid-shaft clavicular fractures with threaded elastic intramedullary nail (TEIN) and elastic locking intramedullary nail (ELIN). *Orthop Surg*. 2021;13(7):2111–2118.
11. **Xing Y**, **Gu Y**, **Xu LC**, **Siedlecki CA**, **Donahue HJ**, **You J**. Effects of membrane cholesterol depletion and GPI-anchored protein reduction on osteoblastic mechanotransduction. *J Cell Physiol*. 2011;226(9):2350–2359.
12. **Yi Q**, **Liu H**, **Feng J**, **et al**. Splicing factor-modulated generation of mechano growth factor regulates physiological processes in osteoblasts under mechanical stimuli. *Cell Adh Migr*. 2019;13(1):322–331.
13. **Wu Y-F**, **Guo H-M**. The effect of corticotomy on the compensatory remodeling of alveolar bone during orthodontic treatment. *BMC Oral Health*. 2021;21(1):134.
14. **Sellei RM**, **Garrison RL**, **Kobbe P**, **Lichte P**, **Knobe M**, **Pape HC**. Effects of near cortical slotted holes in locking plate constructs. *J Orthop Trauma*. 2011;25 Suppl 1:S35–40.
15. **Gao H**, **Huang J**, **Wei Q**, **He C**. Advances in animal models for studying bone fracture healing. *Bioengineering (Basel)*. 2023;10(2):201.
16. **Bologna FA**, **Audenino AL**, **Terzini M**. Bone plates runout prediction through tensile strength and geometric properties for regulatory mechanical testing. *Ann Biomed Eng*. 2024;52(2):239–249.
17. **Viitanen J**, **Quinn R**, **Allen M**, **Broeckx BJG**, **Bartkowiak T**, **Haimel G**. Do locking plugs improve implant strength? Biomechanical comparison of polyaxial locking constructs with and without locking plugs in a fracture gap model. *BMC Vet Res*. 2023;19(1):104.
18. **Percie du Sert N**, **Hurst V**, **Ahluwalia A**, **et al**. The ARRIVE guidelines 2.0: Updated guidelines for reporting animal research. *PLoS Biol*. 2020;18(7):e3000410.
19. **Zhai L**, **Ma XL**, **Jiang C**, **Zhang B**, **Liu ST**, **Xing GY**. Human autologous mesenchymal stem cells with extracorporeal shock wave therapy for nonunion of long bones. *Indian J Orthop*. 2016;50(5):543–550.
20. **Franceschini A**, **Szklarczyk D**, **Frankild S**, **et al**. STRING V9.1: protein-protein interaction networks, with increased coverage and integration. *Nucleic Acids Res*. 2013;41(Database issue):D808–15.
21. **Palukuri MV**, **Marcotte EM**. Super.Complex: a supervised machine learning pipeline for molecular complex detection in protein-interaction networks. *PLoS One*. 2021;16(12):e0262056.
22. **Fitzgerald J**, **Hughes-Fulford M**. Mechanically induced C-fos expression is mediated by cAMP in MC3T3-E1 osteoblasts. *FASEB J*. 1999;13(3):553–557.
23. **Claes L**. Dynamization of fracture fixation: timing and methods. *Unfallchirurg*. 2018;121(1):3–9.
24. **Mohammed D**, **Versaevel M**, **Bruyère C**, **et al**. Innovative tools for mechanobiology: unraveling outside-in and inside-out mechanotransduction. *Front Bioeng Biotechnol*. 2019;7:162.
25. **Naqvi SM**, **McNamara LM**. Stem cell mechanobiology and the role of biomaterials in governing mechanotransduction and matrix production for tissue regeneration. *Front Bioeng Biotechnol*. 2020;8:597661.
26. **Thu MK**, **Kang YS**, **Kwak JM**, **Jo Y-H**, **Han J-S**, **Yeo I-S**. Comparison between bone-implant interfaces of microtopographically modified zirconia and titanium implants. *Sci Rep*. 2023;13(1):11142.
27. **Park SH**, **O'Connor K**, **McKellop H**, **Sarmiento A**. The influence of active shear or compressive motion on fracture-healing. *J Bone Joint Surg Am*. 1998;80-A(6):868–878.
28. **Claes L**, **Recknagel S**, **Ignatius A**. Fracture healing under healthy and inflammatory conditions. *Nat Rev Rheumatol*. 2012;8(3):133–143.
29. **Yu D**, **Huang C**, **Jiang C**, **Zhu H**. Features of a simvastatin-loaded multi-layered co-electrospun barrier membrane for guided bone regeneration. *Exp Ther Med*. 2021;22(1):713.

30. **Lv J**, **Li X**, **Qiu W**, **et al**. Effect of knee osteoarthritis on the postoperative outcome of proximal femoral nail anti-rotation in the treatment of intertrochanteric fractures in the elderly: a retrospective analysis. *BMC Musculoskelet Disord*. 2023;24(1):868.
31. **Kinoshita N**, **Hashimoto Y**, **Yasue N**, **Suzuki M**, **Cristea IM**, **Ueno N**. Mechanical stress regulates epithelial tissue integrity and stiffness through the FGFR/Erk2 signaling pathway during embryogenesis. *Cell Rep*. 2020;30(11):3875–3888.
32. **Zhang M**, **Ishikawa S**, **Inagawa T**, **et al**. Influence of mechanical force on bone matrix proteins in ovariectomised mice and osteoblast-like MC3T3-E1 cells. *In Vivo*. 2017;31(1):87–95.
33. **Shi D**, **Liu X**, **Li X**, **Li T**, **Liu J**, **Wu L**. Yth m^{6}A RNA-binding protein 1 regulates osteogenesis of MC3T3-E1 cells under hypoxia via translational control of thrombospondin-1. *Int J Mol Sci*. 2023;24(2):1741.
34. **Chen X**, **Chen J**, **Xu D**, **Zhao S**, **Song H**, **Peng Y**. On treating senile osteoporosis by regulating MSCs. *BMC Musculoskelet Disord*. 2017;18(1):423.
35. **Chen SN**, **Lam CK**, **Wan Y-W**, **et al**. Activation of PDGFRA signaling contributes to filamin C-related arrhythmogenic cardiomyopathy. *Sci Adv*. 2022;8(8):eabk0052.
36. **Park S-H**, **Sim WY**, **Min B-H**, **Yang SS**, **Khademhosseini A**, **Kaplan DL**. Chip-based comparison of the osteogenesis of human bone marrow- and adipose tissue-derived mesenchymal stem cells under mechanical stimulation. *PLoS One*. 2012;7(9):e46689.
37. **Wong SA**, **Hu DP**, **Slocum J**, **et al**. Chondrocyte-to-osteoblast transformation in mandibular fracture repair. *J Orthop Res*. 2021;39(8):1622–1632.
38. **Aspera-Werz RH**, **Chen T**, **Ehnert S**, **Zhu S**, **Fröhlich T**, **Nussler AK**. Cigarette smoke induces the risk of metabolic bone diseases: transforming growth factor beta signaling impairment via dysfunctional primary cilia affects migration, proliferation, and differentiation of human mesenchymal stem cells. *Int J Mol Sci*. 2019;20(12):2915.
39. **Yang J**, **Gao J**, **Gao F**, **et al**. Extracellular vesicles-encapsulated microRNA-29B-3P from bone marrow-derived mesenchymal stem cells promotes fracture healing via modulation of the PTEN/PI3K/AKT axis. *Exp Cell Res*. 2022;412(2):113026.
40. **Wallace AL**, **Draper ER**, **Strachan RK**, **McCarthy ID**, **Hughes SP**. The vascular response to fracture micromovement. *Clin Orthop Relat Res*. 1994;301:281–290.
41. **Moore DC**, **Leblanc CW**, **Müller R**, **Crisco JJ**, **Ehrlich MG**. Physiologic weight-bearing increases new vessel formation during distraction osteogenesis: a micro-tomographic imaging study. *J Orthop Res*. 2003;21(3):489–496.
42. **Epari DR**, **Duda GN**, **Thompson MS**. Mechanobiology of bone healing and regeneration: in vivo models. *Proc Inst Mech Eng H*. 2010;224(12):1543–1553.
43. **Qi W**, **Feng X**, **Zhang T**, **Wu H**, **Fang C**, **Leung F**. Development and validation of a modularized external fixator for generating standardized fracture healing micromotions in rats. *Bone Joint Res*. 2021;10(11):714–722.
44. **Kuwahara Y**, **Takegami Y**, **Tokutake K**, **et al**. How does intraoperative fracture malalignment affect postoperative function and bone healing following distal femoral fracture? A retrospective multicentre study. *Bone Jt Open*. 2022;3(2):165–172.
45. **Guo A**, **Zheng Y**, **Zhong Y**, **Mo S**, **Fang S**. Effect of chitosan/inorganic nanomaterial scaffolds on bone regeneration and related influencing factors in animal models: a systematic review. *Front Bioeng Biotechnol*. 2022;10:986212. ,

Author information

W. Wu, MD, Orthopaedic Surgeon,
First Teaching Hospital of Tianjin University of Traditional Chinese Medicine, Tianjin, China;
National Clinical Research Center for Chinese Medicine Acupuncture and Moxibustion, Tianjin, China.

Z. Zhao, MD, Orthopaedic Surgeon
Y. Wang, PhD, Orthopaedic Surgeon
M. Liu, MM, Orthopaedic Surgeon
Orthopedic Department, The Fourth Central Clinical School, Tianjin Medical University, Tianjin, China.

G. Zhu, MSA, Research Associate
L. Li, PhD, Researcher, Head of Department
General Clinical Research Center, Anhui Wanbei Coal-Electricity Group General Hospital, Suzhou, China.

Author contributions

W. Wu: Writing – original draft, Writing – review & editing, Conceptualization, Data curation, Validation, Visualization.
Z. Zhao: Funding acquisition, Project administration.
Y. Wang: Project administration, Supervision.
M. Liu: Software.
G. Zhu: Data curation.
L. Li: Funding acquisition, Supervision, Resources.

Z. Zhao and Y. Wang contributed equally to this work.

Y. Wang and L. Li are joint senior authors.

Funding statement

The authors disclose receipt of the following financial or material support for the research, authorship, and/or publication of this article: financial support from the Natural Science Foundation of Tianjin (grant number 21JCYBJC00280) and the Key program of the Health Commission of Anhui Province (grant number AHWJ2022a034), as reported by Z. Zhao and L. Li, respectively.

ICMJE COI statement

Z. Zhao reports financial support from the Natural Science Foundation of Tianjin (grant number 21JCYBJC00280), related to this study. L. Li reports financial support from the Key program of the Health Commission of Anhui Province (grant number AHWJ2022a034), related to this study.

Data sharing

The data that support the findings for this study are available to other researchers from the corresponding author upon reasonable request.

Acknowledgements

The authors thank the Home for Researchers editorial team (https://www.home-for-researchers.com/#/) for their language editing service.

Ethical review statement

A detailed description of all protocols can be found in the Registered Report (https://osf.io/ahmsp; https://doi.org/10.17605/OSF.IO/AHMSP). The study was approved by the animal ethics committee of Anhui Wanbei Coal-Electricity Group General Hospital (WBZY-2023-033).

Open access funding

The authors report that the open access funding for their manuscript was self-funded.